AGU100 ADVANCING EARTH AND SPACE SCIENCE

Geophysical Research Letters

RESEARCH LETTER
10.1029/2019GL084395

Dynamically Triggered Changes of Plate Interface Coupling in Southern Cascadia

Kathryn Materna[1], Noel Bartlow[1], Aaron Wech[2], Charles Williams[3], and Roland Bürgmann[1]

[1]Berkeley Seismology Lab, University of California, Berkeley, CA, USA, [2]U.S. Geological Survey, Alaska Volcano Observatory, Volcano Science Center, Anchorage, AK, USA, [3]GNS Science, Lower Hutt, New Zealand

Key Points:
- GNSS time series near the Mendocino Triple Junction show correlated changes in eastward velocity around the times of nearby $M > 6.5$ earthquakes
- Velocity changes are several mm/yr and are centered updip of the tremor zone
- The observations suggest dynamically triggered coupling changes on the Cascadia subduction interface at about 25 km depth

Supporting Information:
- Supporting Information S1

Correspondence to:
K. Materna,
kmaterna@berkeley.edu

Citation:
Materna, K., Bartlow, N., Wech, A., Williams, C., & Bürgmann, R. (2019). Dynamically triggered changes of plate interface coupling in Southern Cascadia. *Geophysical Research Letters*, *46*, 12,890–12,899. https://doi.org/10.1029/2019GL084395

Received 2 JUL 2019
Accepted 13 OCT 2019
Accepted article online 23 OCT 2019
Published online 21 NOV 2019

Abstract In Southern Cascadia, precise Global Navigation Satellite System (GNSS) measurements spanning about 15 years reveal steady deformation due to locking on the Cascadia megathrust punctuated by transient deformation from large earthquakes and episodic tremor and slip events. Near the Mendocino Triple Junction, however, we recognize several abrupt GNSS velocity changes that reflect a different process. After correcting for earthquakes and seasonal loading, we find that several dozen GNSS time series show spatially coherent east-west velocity changes of ~2 mm/yr and that these changes coincide in time with regional $M > 6.5$ earthquakes. We consider several hypotheses and propose that dynamically triggered changes in megathrust coupling best explain the data. Our inversions locate the coupling changes slightly updip of the tremor-producing zone. We speculate that fluid exchange surrounding the tremor region may be important. Such observations of transient coupling changes are rare and challenging to explain mechanistically but have important implications for earthquake processes on faults.

Plain Language Summary In subduction zones, frictional locking on the subduction interface produces year-by-year surface deformation that is measurable with GPS. During the interseismic period of the earthquake cycle, lasting hundreds of years between major earthquakes, these ground motions are usually constant with time because the locking on the plate interface is relatively unchanging. However, at the Mendocino Triple Junction in Northern California, we find evidence for slight changes in GPS interseismic motion within the last decade that challenge the assumption of constant interseismic deformation. Our results suggest changes in interseismic coupling on the southernmost Cascadia Subduction Zone. Interestingly, these coupling changes appear to be related to large offshore earthquakes and are perhaps triggered by the seismic shaking during those events. These results have important implications for our understanding of seismic hazard in subduction zones.

1. Introduction

In subduction zones, seismically coupled regions of the megathrust accumulate strain during the interseismic period of the seismic cycle. The resulting slip deficit must eventually be released, either through coseismic slip, postseismic slip, or a wide spectrum of recently discovered slow-slip processes such as slow-slip events (SSEs; Bürgmann, 2018; Gomberg et al., 2016; Obara & Kato, 2016). The spatiotemporal evolution of slip deficit (or coupling) is directly related to earthquake and tsunami hazards and thus is important to understand.

SSEs are temporary phenomena. They occur over a range of timescales lasting from weeks to years (e.g., Bartlow et al., 2011; Fu & Freymueller, 2013; Hirose & Obara, 2005; Radiguet et al., 2012), but the subduction interface generally returns to the previous coupling state after SSEs are completed. An SSE may occur spontaneously or be triggered by the passage of regional or teleseismic waves (Araki et al., 2017; Itaba & Ando, 2011; Wallace et al., 2017). However, outside of slow-slip episodes and postseismic slip, fault coupling on the megathrust is often assumed to be constant during the interseismic period.

Here we document observations of abrupt changes in GNSS velocities at the Mendocino Triple Junction (MTJ) of northern California that endure for years, challenging the assumption of constant interseismic coupling. We relate these velocity changes to changes in the state of coupling at the Cascadia Subduction Zone (CSZ) plate interface, separate from the short-term episodic tremor and slip (ETS) events observed in this

region (Brudzinski & Allen, 2007). Unlike typical SSEs, which show a continuous temporal evolution in slip rate, these events show step-like velocity changes that we find coincide closely in time with $M > 6.5$ offshore earthquakes. We interpret our observations as dynamically triggered increases and decreases in plate coupling that endure for years and propose a possible physical mechanism for these changes.

2. Methods

2.1. GNSS Data Processing and Velocity Change Estimation

We analyzed continuous GNSS time series from multiple processing centers and reference frames. We focused on the Plate Boundary Observatory (PBO) combined solutions in the NAM08 reference frame (Herring et al., 2016) and University of Nevada Reno (UNR) Gipsy solutions in the NA12 and IGS08 reference frames (Blewitt et al., 2018), but we also analyzed the PBO Central Washington University (CWU) Gipsy and New Mexico Tech (NMT) GAMIT solutions. Our data set extends through January 2019. For the NMT and PBO combined solutions, we only consider time series through their official end dates in mid-September 2018.

We corrected offsets due to antenna changes and earthquakes by applying offsets from published tables for the NMT, CWU, and PBO solutions (ftp://data-out.unavco.org/pub/products/offset/). For the UNR data, we solved for offsets using mean positions 10 days before and after the provided offset times (http://geodesy.unr.edu/NGLStationPages/steps.txt).

Next, we estimated seasonal and longer-term hydrological corrections for each component of each time series using multiple methodologies (Text S1 in the supporting information). Interannual change in the amplitude or phase of seasonal variation could be important during this period because of the effects of California's drought on GNSS positions from 2011 to 2015 (Argus et al., 2017; Zou et al., 2018). Therefore, we employ a number of physics-based loading models, which include interannual variations, as well as a least squares technique with no interannual variation, to correct for this motion. We also performed a simple correction for 12 ETS offsets in the time series (Text S1).

After removing offsets and seasonal corrections from the time series, we observed consistent velocity changes across much of the MTJ region (Figure 1). We estimated the timing of these changes by looking for "turning points" in the individual low-pass-filtered time series (Text S2). We found that most stations at the MTJ have a turning point within ~60 days of the 2014 and 2016 earthquakes (Figure 2). We then defined four "velocity epochs" for the subsequent analysis based on the occurrence times of the four offshore $M > 6.5$ earthquakes. We excluded 6 months of data after the 2005 and 2010 earthquakes to avoid postseismic transients and 7 days after the 2014 and 2016 earthquakes (Figure 1d and Table S1). Finally, we estimated velocity differences between the four epochs by differencing the slopes of the corrected time series during each epoch. Our procedure for estimating uncertainties of the velocity differences and excluding outlier stations is described in Text S2.

2.2. Tremor Catalog

In order to compare coupling changes with tectonic tremor in space and time, we reevaluated the Pacific Northwest Seismic Network (PNSN) tremor catalog (Wech, 2010) from January 2015 to January 2018. A number of seismic stations in Mendocino became unavailable during mid-2016, requiring a revision of the numerical thresholds used in the tremor detection procedure. Furthermore, we imposed a new detection criterion during this period that decreased the rate of false tremor detections due to spurious data from MTJ stations. Outside of the 2015–2018 window, we used the existing 2012–2019 tremor catalog (Wech, 2010).

2.3. Mechanical Modeling of Velocity Differences

To model the GNSS velocity changes, we performed weighted, constrained least squares inversions using both homogeneous and heterogeneous elastic Green's functions, with and without correcting for ETS offsets. We use nonnegativity constraints for 2016 and nonpositivity constraints (all values restricted to less than zero) for 2014. Weights are the inverse of the uncertainties on the velocity changes, normalized so the average weight is 1. The model fault geometry is a triangular mesh approximation of the McCrory et al. (2012) geometry (Figure 3), with an assumed slip direction fixed on each subfault using the Juan de Fuca-Oregon Coast Block Euler Pole reported in McCaffrey et al. (2007). This Euler Pole implies an east-northeast plate

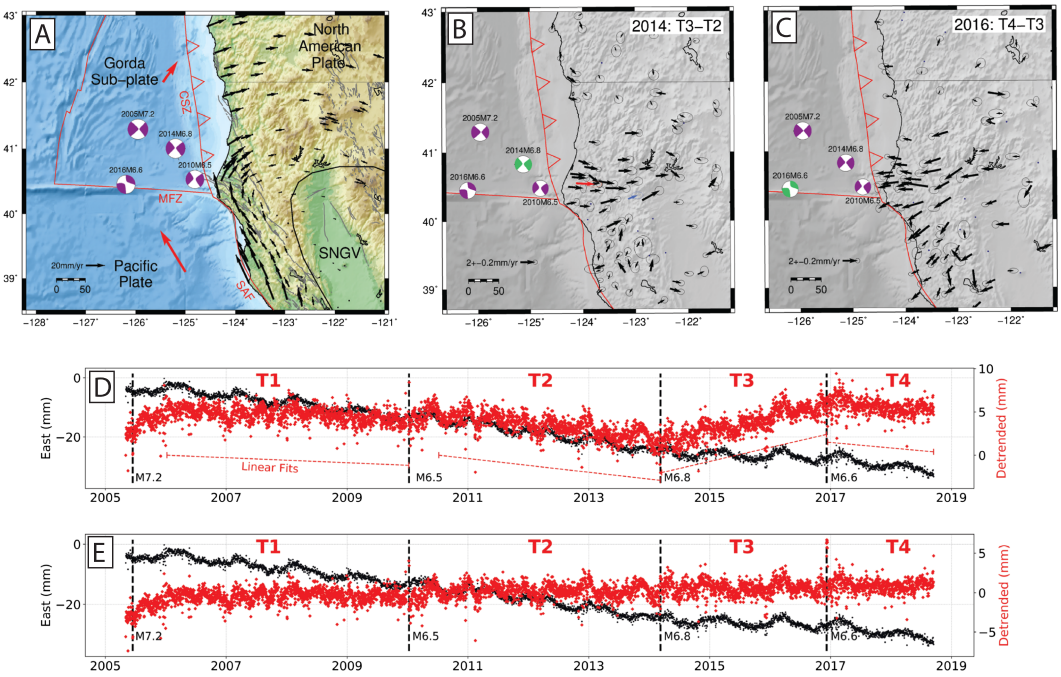

Figure 1. (a) Tectonic setting of the Mendocino Triple Junction, located at the intersection of the San Andreas Fault (SAF), the Mendocino Fault Zone (MFZ), and the Cascadia Subduction Zone (CSZ). The black velocity vectors show the PBO velocity field in the Sierra Nevada Great Valley (SNGV) reference frame, converted using the Euler Pole from Dixon et al. (2000).(b and c) Velocity changes (T3-T2 and T4-T3) from the PBO solutions with least squares seasonal removal, shown with 1-sigma confidence ellipses. (d) Time series of east component for station P160 (red arrow in (b)). Time series after removal of coseismic offsets is shown in black, and the detrended and deseasonalized east component is shown in red, with dashed lines indicating the periods used for slope estimation. (e) Residuals to linear fits in Figure 1d.

convergence at about 31 mm/yr. However, this convergence rate may be inaccurate because it fails to account for internal deformation of the Gorda subplate.

We applied Laplacian smoothing regularization, with the rows of the discrete Laplacian corresponding to each subfault additionally weighted by the inverse of the median value of the Green's functions associated with the subfault. This additional weighting ensures that less resolved subfaults, as indicated by small amounts of surface motion at observable sites, are smoothed more. An additional smoothing parameter

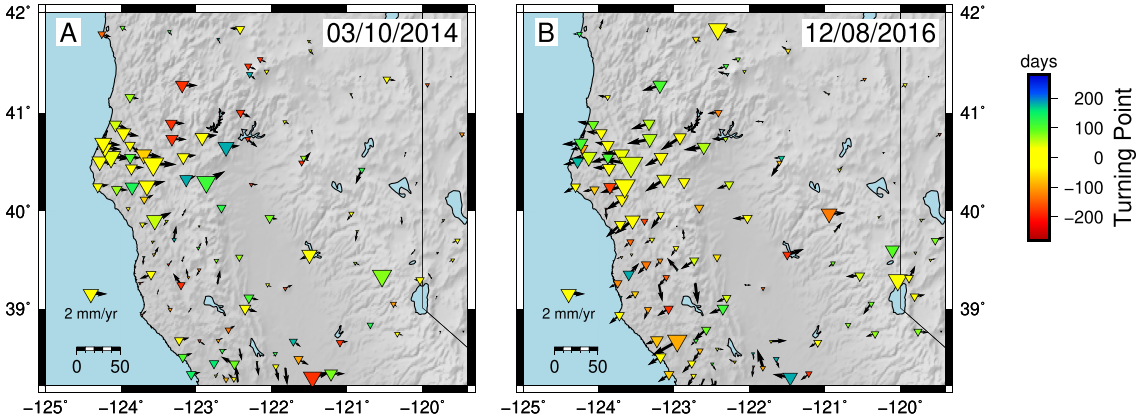

Figure 2. Timing of the slope change in the east component of each station's time series plotted with their velocity changes from Figure 1 (black arrows). Larger triangles represent larger slope changes. A timing value of 0 signifies that the turning point in the detrended time series coincides with the offshore earthquakes in 2014 (A) and 2016 (B); red colors signify times before the earthquake and blue colors after the earthquake.

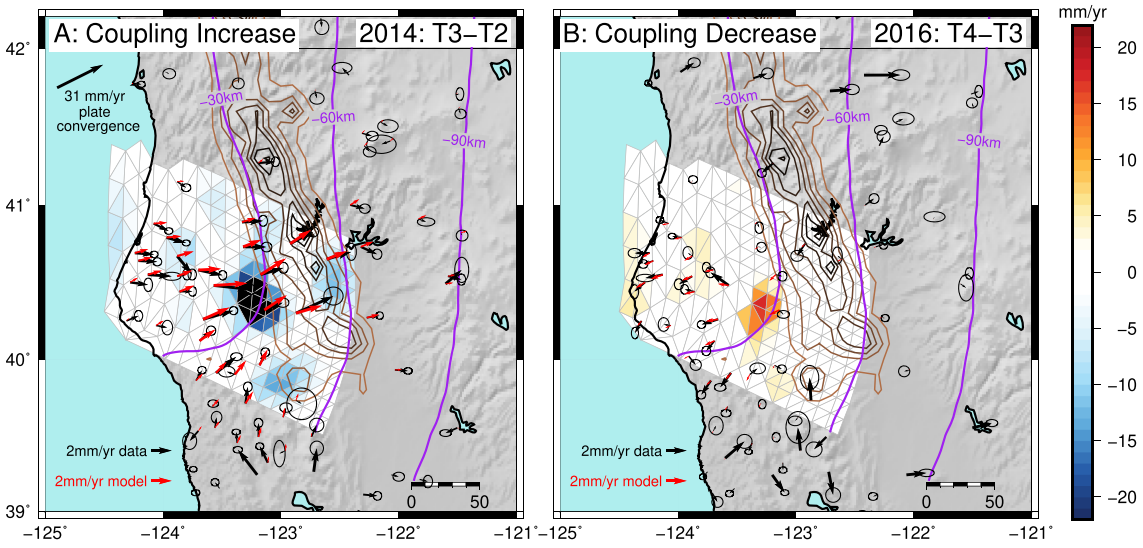

Figure 3. Inversion results for the PBO GNSS velocity changes in 2014 and 2016, using a correction for ETS events, the NLDAS hydrological model to correct for seasonal variation in the time series, and elastic Green's functions computed for a heterogeneous elastic Earth structure. The brown contours represent tremor density from the modified PNSN catalog, ranging from 0 to 2,000 tremor epicenters per 10 × 10 km grid cell. The purple lines show the depth contours of the interface geometry. The most prominent feature is a localized coupling change on the interface around 40.3°N in both inversions.

weights minimizing the Laplacian of the slip distribution relative to fitting the data. This smoothing parameter was chosen via an L-curve analysis, selecting the smoothest model that does not substantially increase the RMS value of the residuals. A parameter value of 800 was chosen for all inversions, although inversions with alternative smoothing parameters are also shown (Figures S18–S20).

Homogeneous Green's functions were calculated using triangular dislocations in an elastic half-space (Thomas, 1993). Heterogeneous Green's functions were calculated using the PyLith finite element software (Aagaard et al., 2013, Aagaard et al., 2017a, 2017b), with density (and by extension, shear modulus) estimated via empirical relationships with V_P and V_S (Brocher, 2005; Stephenson, 2007). The V_P and V_S values were taken from the model of Stephenson (2007) with the V_P and V_S values at 60 km (deepest depth of the model) extended to 400 km depth. Topography is ignored. The mesh used by PyLith to generate the Green's functions is at a much finer resolution than the mesh used in the inversions because PyLith impulses are applied at vertices rather than over a subfault. The PyLith Green's functions are then integrated over each triangular subfault to calculate the heterogenous Green's functions associated with each subfault.

3. Results

We identify three abrupt velocity changes in the cleaned, deseasonalized, and detrended GNSS time series, with the largest of these changes occurring in early 2014 and late 2016. As described in the methods, the onset time of these velocity changes is consistent with the timing of the 2014 and 2016 offshore earthquakes (Figure 2). In the 2-year period starting in early 2014 (time period T3 in Figure 1d), the time series of almost two dozen stations indicate steady eastward velocities that are 2–3 mm/yr larger than in the prior time period T2 (Figure 1b). Unlike typical postseismic transients, this signal does not show significant temporal evolution (Figures 1d and S2). After the 2016 earthquake (time period T4), the eastward velocities reverse some of the velocity change observed in 2014 (Figure 1c). To first order, the results are not sensitive to the technique used for seasonal removal, and the rate changes are visible by eye in many time series prior to any seasonal removal (Figure S1).

After setting aside the 6-month postseismic period following the 2010 earthquake, time period T2 is also associated with a small westward velocity change at about 10 stations at the MTJ (T2 minus T1 in Figure S3a), but these velocity changes are too small to reliably interpret. The 2005 earthquake may have also been associated with local velocity changes. However, only a few stations were installed prior to this earthquake and none

have more than a year of data before the event, so we are unable to estimate these velocity changes. Instead, we focus on understanding the larger velocity changes in 2014 and 2016.

Inverting the observed velocity changes for coupling changes on the plate interface indicates that the 2014 velocity change was associated with a coupling increase, while the 2016 velocity change was associated with a coupling decrease (Figure 3). The coupling change distributions for the 2014 and 2016 events are similar spatially, although with different amplitudes and signs. The coupling changes are predominantly concentrated in a single "spot" on the plate interface near 40.3°N, 123.3°W, located at about 25–28 km depth just updip of the main ETS zone. Our preferred model (Figure 3) utilizes heterogeneous Green's functions with ETS corrections and NLDAS hydrological corrections (Mitchell, 2004; Puskas et al., 2017; Text S1), but alternative inversions show the same coupling change patch (Figures S7 and S8). Inversions performed with a shallower interface place the coupling patch in the same location but reduce its amplitude. Additionally, small patches of coupling change exist updip from the main spot to fit observed velocity changes at coastal stations. A plate velocity increase of 25 mm/yr in the dominant coupling change patch, or approximately 80% of the estimated plate convergence rate, is required to fit velocity change in 2014. In 2016, the required plate interface slip rate decrease is about 15 mm/yr in the same area.

4. Alternative Explanations for Observed Velocity Changes

We consider five hypotheses to explain the coherent GNSS velocity changes following the 2014 and 2016 earthquakes: coseismic static stress changes on the CSZ, afterslip or viscoelastic relaxation, reference frame instability, multiannual hydrological loading, and coupling changes on the megathrust.

We reject explanations involving static stress changes because of the amplitude of the stresses. Static stresses could hypothetically increase the coupling by increasing the fault-normal stress or by decreasing the shear stresses driving slip on the interface. However, Coulomb stress changes from a single-dislocation model of the 2014 event are only ~200 Pa at the position of the largest velocity changes, although in the right direction to produce increased coupling on the interface (Figure S11). For the 2016 event, the predicted coseismic Coulomb stress changes are less than 10 Pa and in the wrong direction. In addition, Coulomb stress changes are larger closer to the earthquakes in regions that did not experience velocity changes.

We also reject a hypothesis involving viscoelastic relaxation or afterslip following the offshore earthquakes because it cannot explain the largest displacements occurring inland from the coast rather than close to the earthquakes. Deep afterslip is similarly unable to explain the spatial gradients of the 2014 observations and the directions of the 2016 observations (Figure S12). These hypotheses also do not explain the apparent steady velocities after the 2014 and 2016 earthquakes, as afterslip and viscoelastic relaxation both typically feature a decaying temporal evolution.

Multiannual hydrology (e.g., Argus et al., 2017) or reference frame instability (e.g., Tian & Shen, 2016) may play a role in generating large-scale motions in the GNSS network. Reference frame instability is unlikely given the stability of nearby stations in Oregon (Figure S3). Multiannual hydrology, however, must be carefully considered in light of California's drought from 2011 to 2015. The elastic-loading-induced horizontal velocity changes expected from several hydrological loading models (Text S1) are not sufficient to explain the signals we observe. We find that the predicted horizontal rate changes due to these hydrological models are generally in the same direction as the observed velocity changes but are only 10–50% of the amplitude in Mendocino and extend over a much wider region from central California across Oregon (Figures S3–S6). Predictions from GRACE differ from the other models in their orientations and low amplitudes (Figure S6), which reflects the low spatial resolution of the GRACE-derived load distribution. Beyond elastic loading, the poroelastic effects of aquifer recharge during drought recovery could produce horizontal motions near the edge of groundwater basins (Bawden et al., 2001) but could not produce changes on the large scales observed in Mendocino. Poroelastic deformation may, however, be responsible for some of the rate changes we see at stations near large sedimentary basins in central California. We document the full regional pattern of velocity changes in Figures S3–S5 and Text S3.

In light of the closely coincident timing of the velocity changes and the nearby $M6.5$–$M7.2$ main shocks, we consider changes in coupling on the interface between the subducting Gorda subplate and the fore-arc blocks to be the most likely explanation for the observations at the MTJ. This hypothesis implies that

plate interface coupling increased during the period from March 2014 to December 2016 and then decreased after December 2016.

5. Discussion

The location of inferred coupling changes is updip of the ETS zone (Michel et al., 2018; Wech, 2010; Wech & Creager, 2011) and downdip of the locked plate interface of the Cascadia megathrust (Wang & Tréhu, 2016). Little is known about this region in Cascadia, or the so-called "gap" (Hyndman, 2013). Interseismic coupling models show low average coupling in this region ranging from 0% to 30% (Schmalzle et al., 2014). In other warm-slab subduction zones such as Nankai, this region hosts long-term SSEs that are distinct from the deeper and shorter-duration ETS events (Obara & Kato, 2016) and may involve either frictional or viscous deformation mechanisms (Gao & Wang, 2017). In Cascadia, such long-term SSE phenomena have been hypothesized (Wech & Creager, 2011) but are yet undocumented. The coupling changes documented here may reflect a similar long-term variation in slip behavior of the gap, although unlike a traditional SSE, there is no observable temporal evolution to our identified signals. While we do not estimate absolute slip velocity on the plate interface, estimated velocity changes are below the plate rate in both of our inversions, suggesting a coupling change rather than a SSE.

In light of the temporal association with nearby earthquakes, we suspect that the coupling changes somehow respond to dynamic stress perturbations. Seismic data show that the 2014 and 2016 earthquakes had similar shaking amplitudes and presumably similar dynamic stresses in the region of the coupling change in the long-period bands thought to be important for earthquake triggering (Brodsky & Prejean, 2005; Figures S15–S17). The 2016 event created especially large Love waves for its magnitude, perhaps allowing it to influence coupling at such large distances (Figure S15). Unfortunately, using only surface measurements, it is extremely difficult to quantify the dynamic stresses applied to the interface at depth. This is especially true given our inability to estimate any waveguide effects of a finite width shear or damage zone at the interface.

One possible mechanism for dynamically triggered coupling changes is to alter the physical properties of the interface itself, such as the frictional contact area or rate-and-state friction parameters, through dynamic shaking. Experimentally, dynamic shaking has been observed to change frictional contacts in granular materials and fault gouge (Johnson et al., 2008). Observational studies suggest that dynamic triggering of earthquakes or tremor is most likely when low-frequency surface waves interact with faults at very low effective normal stresses (Brodsky & Prejean, 2005; Miyazawa et al., 2008). However, these experiments typically move the faults closer to failure through dynamic shaking rather than providing mechanisms for both coupling increases and decreases under similar levels of shaking.

We instead propose an explanation involving pore fluid pressure exchange between the ETS zone and the coupling change zone just updip. ETS zones worldwide are thought to host nearly lithostatic pore fluid pressures and thus low effective normal stresses (Matsubara et al., 2009; Shelly et al., 2007). These areas may undergo cyclic pressure changes during ETS cycles (Nakajima & Uchida, 2018; Warren-Smith et al., 2019). A low-permeability seal above the ETS zone may control the recurrence interval of ETS and the diffusion of fluids away from the overpressured ETS zone (Audet & Bürgmann, 2014). If this seal is fractured during dynamic shaking, or old fractures are reactivated, fracture permeability may temporarily increase, allowing pressure-driven flow across the boundary and rapid pressure equalization with a high pore fluid pressure zone located updip of the seal. Depending on the timing of the shaking with respect to the most recent ETS events, and the relative pressure in the updip zone, the unsealing could result in pressure diffusing into or out of the ETS zone, allowing for coupling in the updip region to increase or decrease (Figure 4). A similar model of permanent pressure changes through fracturing of low-permeability seals has been proposed for groundwater wells in Oregon following teleseismic shaking (Brodsky et al., 2003). This hypothesis requires that fluids are additionally confined by a seal mechanism updip from the ETS zone, creating a high pore pressure region corresponding to the coupling change "spot" in this location. Speculatively, the coupling change zone's location may be controlled by the plate interface geometry, which shows a distinct "bump" in this region as indicated by the bend in the 30 km contour in Figure 3.

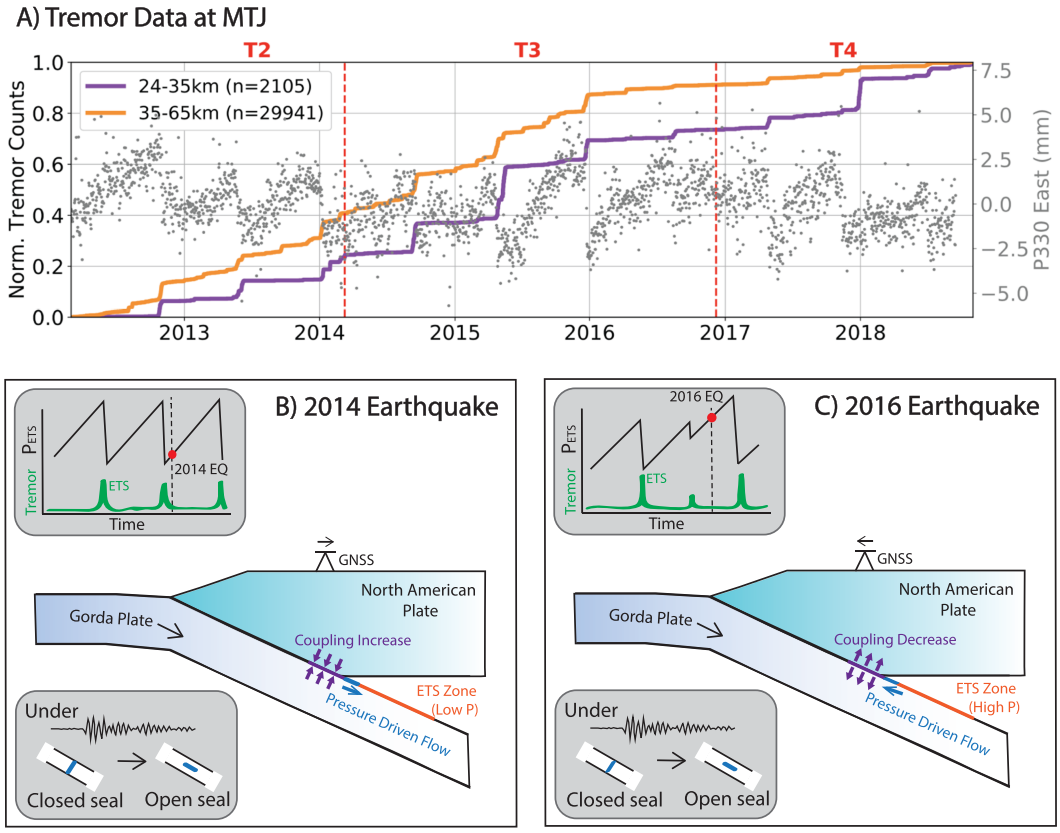

Figure 4. (a) Tremor as a function of time in the MTJ, focusing on the region between 40°N and 41°N in the reprocessed tremor catalog. The detrended and seasonal-removed east component time series for station P330, located above the tremor zone at 40.3°N (blue arrow in Figure 1b), is plotted with gray dots. (b and c) Cartoon schematic showing pressure conditions on the interface at the time of the 2014 and 2016 earthquakes.

We hypothesize that coupling increased updip of the ETS zone after the 2014 earthquake because the dynamic shaking occurred shortly after an ETS event (Figure 4), when the pore pressure in the ETS zone was lowest. If the pressure seal was fractured during shaking, fluids could move into the ETS zone from the updip high-pressure reservoir, increasing coupling in the updip region. The 2016 event occurred 3 months after a major ETS event to the north but that ETS event did not produce much tremor in the MTJ region (Figure S13). It is therefore possible that pressures were still increasing in the ETS zone downdip of the observed coupling change, where the previous large ETS occurred ~12 months before. Fracturing the seal in 2016 could have allowed fluids to diffuse in the opposite direction, decreasing coupling updip (Figure 4). Similar to the 2016 earthquake, the 2010 earthquake occurred late in an ETS cycle and produced velocity changes, although smaller and more difficult to resolve, in the same direction as the 2016 case (Figure S3). Although we propose a mechanism that invokes fluid flow within the fault zone, any mechanism producing increases and decreases of effective normal stress updip of the ETS zone (such as fluid exchange with the subducted slab, or overriding crust, or the adjacent subduction interface) could also contribute to the velocity change phenomena.

Coupling changes similar to the MTJ have been observed in several subduction zones in other parts of the world. The closest analogue to the Mendocino case was observed south of the Iquique earthquake in Chile, where interface coupling appeared to increase after the earthquake on a distant enough part of the plate interface to preclude static triggering (Hoffmann et al., 2018). Several other changes in megathrust coupling have been observed in Chile and are potentially also associated with earthquakes (Jara et al., 2017; Klein et al., 2018; Melnick et al., 2017). Transients in GNSS velocities in northeast Japan have also been documented and suggested to reflect coupling changes, although they may represent a different process (Heki & Mitsui, 2013; Mavrommatis et al., 2014). Elsewhere, a long-lived decrease in coupling was documented in Sumatra using campaign measurements following an earthquake in 2000

(Prawirodirdjo et al., 2010). In south central Alaska, multiple coupling changes were observed during the past two decades associated with many-years-long SSEs (Li et al., 2016). To our knowledge, the MTJ case represents the first example of dynamic stressing leading to both increases and decreases in coupling on the same fault region.

Interseismic coupling models are a key element in our understanding of subduction zone processes and associated hazards. However, coupling models typically consider coupling to be time independent and not susceptible to dynamic strain transients. In light of these observations, it may be necessary instead to consider interseismic coupling in these models as a time-average quantity with potentially substantial temporal variations. The time-dependent coupling changes inferred at the MTJ in this study and elsewhere have significant implications for our understanding of subduction zones and should be the subject of further work in the future.

6. Conclusions

We observe changes in GNSS velocities in northern California that depict a consistent increased eastward movement of several mm/yr after mid-2014 and a westward reversal after late 2016. We invert these observations to model coupling changes on the CSZ, and we find that interseismic coupling updip of the ETS zone increased by ~80% (25 mm/yr) at the time of a *M*6.8 earthquake in 2014 and then decreased again by ~50% following an *M*6.6 event in 2016. These observations suggest that at least in the southernmost CSZ, interplate coupling is a time-dependent quantity on years-long timescales in addition to the short timescales of ETS events. We infer that both coupling increases and decreases can result from dynamic stressing by nearby large earthquakes, which we propose reflects variable pressure gradients in the fault zone at the time of the triggering events. Subduction zone coupling models, which are critical for estimating the hazards posed by megathrust earthquakes, are usually made under the assumption that interseismic coupling is time independent. Our findings suggest that this assumption may not hold in all regions or periods even outside of the ETS zone. This finding has direct implications for our understanding of earthquakes in Cascadia and elsewhere.

Acknowledgments
We are very grateful for GNSS data from multiple processing centers (PBO, UNR, NMT, and CWU). The PBO and NLDAS data are provided by the UNAVCO facility with support from the National Science Foundation (NSF) and National Aeronautics and Space Administration (NASA) under NSF Cooperative Agreement EAR-0735156. We thank the editor and two anonymous reviewers whose comments greatly improved the manuscript. The tremor catalog produced as part of this project is available at Wech (2019). The GRACE data set is the monthly land water mass grids, NETCDF Release 5.0 Ver. 5.0. PO.DAAC, CA, USA, accessed 2018-07-01. We acknowledge support by the NSF Graduate Research Fellowship Program and NSF awards EAR-1841371 and OCE-1905098. Any use of trade, firm, or product names is for descriptive purposes only and does not imply endorsement by the U.S. Government.

References

Aagaard, B. T., Knepley, M. G., & Williams, C. A. (2013). A domain decomposition approach to implementing fault slip in finite-element models of quasi-static and dynamic crustal deformation. *Journal of Geophysical Research: Solid Earth*, *118*, 3059–3079. https://doi.org/10.1002/jgrb.50217

Aagaard, B. T., Knepley, M. G., & Williams, C. A. (2017a). PyLith User Manual, Version 2.2.1. Davis, CA.

Aagaard, B. T., Knepley, M. G., & Williams, C. A. (2017b). PyLith v2.2.1. In *Computational Infrastructure of Geodynamics*. Davis, CA. https://doi.org/10.5281/zenodo.886600

Araki, E., Saffer, D. M., Kopf, A. J., Wallace, L. M., Kimura, T., Machida, Y., et al. (2017). Recurring and triggered slow-slip events near the trench at the Nankai Trough subduction megathrust. *Science*, *356*(6343), 1157–1160. https://doi.org/10.1126/science.aan3120

Argus, D. F., Landerer, F. W., Wiese, D. N., Martens, H. R., Yuning, F., Famiglietti, J. S., et al. (2017). Sustained water loss in California's mountain ranges during severe drought from 2012 to 2015 inferred from GPS. *Journal of Geophysical Research: Solid Earth*, *122*, 10,559–10,585. https://doi.org/10.1002/2017JB014424

Audet, P., & Bürgmann, R. (2014). Possible control of subduction zone slow-earthquake periodicity by silica enrichment. *Nature*, *510*(7505), 389–392. https://doi.org/10.1038/nature13391

Bartlow, N. M., Miyazaki, S.'. I., Bradley, A. M., & Segall, P. (2011). Space-time correlation of slip and tremor during the 2009 Cascadia slow slip event. *Geophysical Research Letters*, *38*, L18309. https://doi.org/10.1029/2011GL048714

Bawden, G. W., Thatcher, W., Stein, R. S., Hudnut, K. W., & Peltzer, G. (2001). Tectonic contraction across Los Angeles after removal of groundwater pumping effects. *Nature*, *412*(6849), 812–815. https://doi.org/10.1038/35090558

Blewitt, G., Hammond, W. C., & Kreemer, C. (2018). Harnessing the GPS data explosion for interdisciplinary science. *Eos*, *99*. https://doi.org/https://doi.org/10.1029/2018EO104623

Brocher, T. M. (2005). Empirical relations between elastic wavespeeds and density in the Earth's crust. *Bulletin of the Seismological Society of America*, *95*(6), 2081–2092. https://doi.org/10.1785/0120050077

Brodsky, E. E., & Prejean, S. G. (2005). New constraints on mechanisms of remotely triggered seismicity at Long Valley Caldera. *Journal of Geophysical Research*, *110*, B04302. https://doi.org/10.1029/2004JB003211

Brodsky, E. E., Roeloffs, E., Woodcock, D., Gall, I., & Manga, M. (2003). A mechanism for sustained groundwater pressure changes induced by distant earthquakes. *Journal of Geophysical Research*, *108*(B8), 2390. https://doi.org/10.1029/2002JB002321

Brudzinski, M. R., & Allen, R. M. (2007). Segmentation in episodic tremor and slip all along Cascadia. *Geology*, *35*(10), 907–910. https://doi.org/10.1130/G23740A.1

Bürgmann, R. (2018). The geophysics, geology and mechanics of slow fault slip. *Earth and Planetary Science Letters*, *495*, 112–134. https://doi.org/10.1016/j.epsl.2018.04.062

Dixon, T. H., Miller, M., Farina, F., Wang, H., & Johnson, D. (2000). Present-day motion of the Sierra Nevada Block and some tectonic implications for the Basin and Range Province, North American Cordillera. *Tectonics*, *19*(1), 1–24. https://doi.org/10.1029/1998TC001088

Fu, Y., & Freymueller, J. T. (2013). Repeated large slow slip events at the Southcentral Alaska Subduction Zone. *Earth and Planetary Science Letters*, *375*, 303–311. https://doi.org/10.1016/j.epsl.2013.05.049

Gao, X., & Wang, K. (2017). Rheological separation of the megathrust seismogenic zone and episodic tremor and slip. *Nature*, *543*(7645), 416–419. https://doi.org/10.1038/nature21389

Gomberg, J., Wech, A., Creager, K., Obara, K., & Agnew, D. (2016). Reconsidering earthquake scaling. *Geophysical Research Letters*, *43*, 6243–6251. https://doi.org/10.1002/2016GL069967

Heki, K., & Mitsui, Y. (2013). Accelerated Pacific Plate subduction following interplate thrust earthquakes at the Japan Trench. *Earth and Planetary Science Letters*, *363*, 44–49. https://doi.org/10.1016/j.epsl.2012.12.031

Herring, T. A., Melbourne, T. I., Murray, M. H., Floyd, M. A., Szeliga, W. M., King, R. W., et al. (2016). Plate Boundary Observatory and related networks: GPS data analysis methods and geodetic products. *Reviews of Geophysics*, *54*, 759–808. https://doi.org/10.1002/2016RG000529

Hirose, H., & Obara, K. (2005). Repeating short- and long-term slow slip events with deep tremor activity around Bungo Channel Region, Southwest Japan. *Earth, Planets and Space*, *57*, 961–972.

Hoffmann, F., Metzger, S., Moreno, M., Deng, Z., Sippl, C., Ortega-Culaciati, F., & Oncken, O. (2018). Characterizing afterslip and ground displacement rate increase following the 2014 Iquique-Pisagua M_w8.1 earthquake, Northern Chile. *Journal of Geophysical Research: Solid Earth*, *123*, 4171–4192. https://doi.org/10.1002/2017JB014970

Hyndman, R. D. (2013). Downdip landward limit of Cascadia great earthquake rupture. *Journal of Geophysical Research: Solid Earth*, *118*, 5530–5549. https://doi.org/10.1002/jgrb.50390

Itaba, S., & Ando, R. (2011). A slow slip event triggered by teleseismic surface waves. *Geophysical Research Letters*, *38*, L21306. https://doi.org/10.1029/2011GL049593

Jara, J., Socquet, A., Marsan, D., & Bouchon, M. (2017). Long-term interactions between intermediate depth and shallow seismicity in North Chile subduction zone. *Geophysical Research Letters*, *44*, 9283–9292. https://doi.org/10.1002/2017GL075029

Johnson, P. A., Savage, H., Knuth, M., Gomberg, J., & Marone, C. (2008). Effects of acoustic waves on stick-slip in granular media and implications for earthquakes. *Nature*, *451*(7174), 57–60. https://doi.org/10.1038/nature06440

Klein, E., Duputel, Z., Zigone, D., Vigny, C., Boy, J. P., Doubre, C., & Meneses, G. (2018). Deep transient slow slip detected by survey GPS in the region of Atacama, Chile. *Geophysical Research Letters*, *45*, 12,263–12,273. https://doi.org/10.1029/2018GL080613

Li, S., Freymueller, J., & McCaffrey, R. (2016). Slow slip events and time-dependent variations in locking beneath Lower Cook Inlet of the Alaska-Aleutian Subduction Zone. *Journal of Geophysical Research: Solid Earth*, *121*, 1060–1079. https://doi.org/10.1002/2015JB012491

Matsubara, M., Obara, K., & Kasahara, K. (2009). High-VP/VS zone accompanying non-volcanic tremors and slow-slip events beneath Southwestern Japan. *Tectonophysics*, *472*(1–4), 6–17. https://doi.org/10.1016/j.tecto.2008.06.013

Mavrommatis, A., Segall, P., & Johnson, K. M. (2014). A decadal-scale deformation transient prior to the 2011 M_w9.0 Tohoku-Oki earthquake. *Geophysical Research Letters*, *41*, 4486–4494. https://doi.org/10.1002/2014GL060139

McCaffrey, R., Qamar, A. I., King, R. W., Wells, R., Khazaradze, G., Williams, C. A., et al. (2007). Fault locking, block rotation and crustal deformation in the Pacific Northwest. *Geophysical Journal International*, *169*(3), 1315–1340. https://doi.org/10.1111/j.1365-246X.2007.03371.x

McCrory, P. A., Luke Blair, J., Waldhauser, F., & Oppenheimer, D. H. (2012). Juan de Fuca slab geometry and its relation to Wadati-Benioff Zone seismicity. *Journal of Geophysical Research*, *117*, B09306. https://doi.org/10.1029/2012JB009407

Melnick, D., Moreno, M., Quinteros, J., Baez, J. C., Deng, Z., Li, S., & Oncken, O. (2017). The super-interseismic phase of the megathrust earthquake cycle in Chile. *Geophysical Research Letters*, *44*, 784–791. https://doi.org/10.1002/2016GL071845

Michel, S., Gualandi, A., & Avouac, J.-P. (2018). Interseismic coupling and slow slip events on the Cascadia megathrust. *Pure and Applied Geophysics*, *176*(10), 4641–4642. https://doi.org/10.1007/s00024-018-2006-7

Mitchell, K. E. (2004). The multi-institution North American Land Data Assimilation System (NLDAS): Utilizing multiple GCIP products and partners in a continental distributed hydrological modeling system. *Journal of Geophysical Research*, *109*, D07S90. https://doi.org/10.1029/2003JD003823

Miyazawa, M., Brodsky, E. E., & Mori, J. (2008). Learning from dynamic triggering of low-frequency tremor in subduction zones. *Earth, Planets and Space*, *60*(10), e17–e20. https://doi.org/10.1186/BF03352858

Nakajima, J., & Uchida, N. (2018). Repeated drainage from megathrusts during episodic slow slip. *Nature Geoscience*, *11*(5), 351–356. https://doi.org/10.1038/s41561-018-0090-z

Obara, K., & Kato, A. (2016). Connecting slow earthquakes to huge earthquakes. *Science*, *353*(6296), 253–257. https://doi.org/10.1126/science.aaf1512

Prawirodirdjo, L., McCaffrey, R., Chadwell, D., Bock, Y., & Subarya, C. (2010). Geodetic observations of an earthquake cycle at the Sumatra Subduction Zone: Role of interseismic strain segmentation. *Journal of Geophysical Research*, *115*, B03414. https://doi.org/10.1029/97GL52691

Puskas, C. M., Meertens, C. M., & Phillips, D. (2017). Hydrologic loading model displacements from the National and Global Data Assimilation Systems (NLDAS and GLDAS). https://www.unavco.org/data/gps-gnss/associated-products/hydrological/displacement-model-readme.pdf.

Radiguet, M., Cotton, F., Vergnolle, M., Campillo, M., Walpersdorf, A., Cotte, N., & Kostoglodov, V. (2012). Slow slip events and strain accumulation in the Guerrero Gap, Mexico. *Journal of Geophysical Research*, *117*, B04305. https://doi.org/10.1029/2011JB008801

Schmalzle, G. M., McCaffrey, R., & Creager, K. C. (2014). Central Cascadia subduction zone creep. *Geochemistry, Geophysics, Geosystems*, *15*, 1515–1532. https://doi.org/10.1002/2013GC005172

Shelly, D. R., Beroza, G. C., & Ide, S. (2007). Non-volcanic tremor and low-frequency earthquake swarms. *Nature*, *446*(7133), 305–307. https://doi.org/10.1038/nature05666

Stephenson, W. J. (2007). Velocity and density models incorporating the Cascadia subduction zone for 3D earthquake ground motion simulations.

Thomas, A. L. (1993). Poly3D: A three-dimensional, polygonal element, displacement discontinuity boundary element computer program with applications to fractures, faults, and cavities in the Earth's crust. Stanford University.

Tian, Y., & Shen, Z. K. (2016). Extracting the regional common-mode component of GPS station position time series from dense continuous network. *Journal of Geophysical Research: Solid Earth*, *121*, 1080–1096. https://doi.org/10.1002/2015JB012253

Wallace, L. M., Kaneko, Y., Hreinsdóttir, S., Hamling, I., Peng, Z., Bartlow, N., et al. (2017). Large-scale dynamic triggering of shallow slow slip enhanced by overlying sedimentary wedge. *Nature Geoscience*, *10*(10), 765–770. https://doi.org/10.1038/ngeo3021

Wang, K., & Tréhu, A. M. (2016). Some outstanding issues in the study of great megathrust earthquakes—The Cascadia example. *Journal of Geodynamics*, *98*, 1–18. https://doi.org/10.1016/j.jog.2016.03.010

Warren-Smith, E., Fry, B., Wallace, L., Chon, E., Henrys, S., Sheehan, A., et al. (2019). Episodic stress and fluid pressure cycling in subducting oceanic crust during slow slip. *Nature Geoscience*, *12*(6), 475–481. https://doi.org/10.1038/s41561-019-0367-x

Wech, A. (2019). Tremor detections near the Mendocino Triple Junction, 2015–2018, Mendeley Data, V1. https://doi.org/10.17632/znmyb9snny.1

Wech, A. G. (2010). Interactive tremor monitoring. *Seismological Research Letters*, *81*(4), 664–669. https://doi.org/10.1785/gssrl.81.4.664

Wech, A. G., & Creager, K. C. (2011). A continuum of stress, strength and slip in the Cascadia subduction zone. *Nature Geoscience*, *4*(9), 624–628. https://doi.org/10.1038/ngeo1215

Zou, Z., Xiao, X., Dong, J., Qin, Y., Doughty, R. B., Menarguez, M. A., et al. (2018). Divergent trends of open-surface water body area in the Contiguous United States from 1984 to 2016. *Proceedings of the National Academy of Sciences*, *115*(15), 201719275. https://doi.org/10.1073/pnas.1719275115